



HAL
open science

Determination of fast neutron RBE using a fully mechanistic computational model

Azam Zabihi, John Tello, Sebastien Incerti, Ziad Francis, Ghasem Forozani, Farid Semsarha, Amir Moslehi, Mario A. Bernal

► **To cite this version:**

Azam Zabihi, John Tello, Sebastien Incerti, Ziad Francis, Ghasem Forozani, et al.. Determination of fast neutron RBE using a fully mechanistic computational model. *Appl.Radiat.Isot.*, 2020, 156, pp.108952. 10.1016/j.apradiso.2019.108952 . hal-02467218

HAL Id: hal-02467218

<https://hal.science/hal-02467218>

Submitted on 7 May 2020

HAL is a multi-disciplinary open access archive for the deposit and dissemination of scientific research documents, whether they are published or not. The documents may come from teaching and research institutions in France or abroad, or from public or private research centers.

L'archive ouverte pluridisciplinaire **HAL**, est destinée au dépôt et à la diffusion de documents scientifiques de niveau recherche, publiés ou non, émanant des établissements d'enseignement et de recherche français ou étrangers, des laboratoires publics ou privés.

Determination of fast neutron RBE using a fully mechanistic computational model

Azam Zabihi

Department of Physics, Faculty of Science, Bu-Ali Sina University, Hamedan, Iran.

John Tello

Instituto de Física Gleb Wataghin. Universidade Estadual de Campinas. Brazil.

Sebastien Incerti

University of Bordeaux, CENBG, UMR 5797, F-33170 Gradignan, France

Ziad Francis

Université Saint Joseph, Faculty of Sciences, Department of Physics, Beirut, Lebanon.

Ghasem Forozani

Department of Physics, Payame Noor University, P.O. Box 19395-3697, Tehran, Iran.

Farid Semsarha

Institute of Biochemistry and Biophysics (IBB), University of Tehran, P.O. Box: 13145-1384, Tehran, Iran.

Amir Moslehi

Radiation Applications Research School, Nuclear Science and Technology Research Institute, P.O. Box: 11365-3486, Tehran, Iran.

Mario.A. Bernal

Instituto de Física Gleb Wataghin. Universidade Estadual de Campinas. Brazil.

Abstract

This work presents a model previously developed for estimating relative biological effectiveness (RBE) associated with high-LET particles. It is based on the combination of Monte Carlo simulations of particle interactions when traversing an atomic resolution DNA geometrical model. In addition, the model emulates the induction of lethal damage from the interaction of two sublethal lesions, taken as double-strand breaks. The Geant4-DNA package was used for simula-

tions with liquid water as the transport medium. The RBE of neutron beams with energies ranging from 0.1 MeV up to 14 MeV was studied. The model succeeded in reproducing the general behavior of RBE as a function of neutron energy, including the RBE peak reported by experiments at approximately 0.4 MeV. Furthermore, the results of the model agree rather well with some experimental works. However, our results underestimate RBE for neutron energies above approximately 5 MeV due to the current limitations of Geant4-DNA for the tracking of heavy ions below 0.5 MeV/u.

Keywords: Monte Carlo, Radiobiology, neutron, RBE

1. Introduction

Interaction of ionizing particles with living beings induces molecular damage, such as single and double DNA strand breaks, which may lead to biological effects like affecting genome and cancer [1, 2, 3, 4]. Biological effects induced by fast neutrons have been studied since the use of atomic bombs in Japan [5, 6, 7, 8]. Since then, this interest has spread to other fields. Fast neutron beams have been used for cancer therapy at various facilities around the world [9, 10, 11, 12, 13, 14, 15, 16]. In addition, this problem is of interest for radiation risk assessment for nuclear power plant workers as well as for astronauts during long manned space missions [17, 18, 19, 20]. Neutrons have higher relative biological effectiveness (RBE) than low linear energy transfer (LET) radiation. This is a prominent issue in studies of mechanisms for cancer induction in humans at low doses and low dose rates from neutrons [21]. Many studies on fast neutron RBE have been performed. This work refers to the most relevant works found in the literature. Zabihi et al. [22] proposed an approach to estimate RBE of fast neutrons with energies ranging from 0.1 MeV to 14 MeV using the Geant4 toolkit. This approach used an atomic resolution DNA geometrical model extracted from the Protein Data Bank. They succeeded in reproducing the behavior of the RBE and the RBE_{max} as a function of the incident neutron energy. Baiocco et al. [23] reported neutron biological effectiveness for a wide

range of initial neutron energy (0.0625–64 MeV/u) with the PHITS (Particle and Heavy Ion Transport) and PARTRAC (PARTicles TRACks) Monte Carlo
45 codes. They investigated how neutron energy influences some microdosimetric quantities. In addition, they estimated RBE of neutrons, using the induction of double-strand break (DSB) clusters as biological endpoint. Stewart et al. [24] used the same biological endpoint for estimating neutron RBE but using different MC code and biophysical model. Ottolenghi et al. [25] estimated the
50 relative risk of damage induction by neutrons compared with photons. Schmid et al. experimentally studied the capacity of nearly monoenergetic neutrons at energies in the ranges of 36 keV–15.0 MeV [21] and 565 keV [26] for induction of dicentrics in human lymphocytes. Tanaka et al. [27] also carried out experiments to investigate biological effects induced by monoenergetic neutrons
55 with energies ranging from 0.186 MeV up to 2.3 MeV and ^{252}Cf neutrons on human lymphocytes, which are related to Hiroshima atomic bomb radiation. Pandita et al. [28] studied the impact of monoenergetic neutrons with energies in the range of 0.22–13.6 MeV on normal human fibroblasts. They reported RBE for neutrons relative to ^{60}Co γ -rays, ^{137}Cs γ -rays, and kV X-rays. Miller
60 et al. [29] determined RBE for cell survival and neoplastic transformation for fast neutrons with energies from 0.040 MeV to 13.7 MeV. Their RBE results for both biological endpoints were similar. Warenius et al. [30] studied RBE of fast neutrons for apoptosis of mouse thymocytes. The use of neutrons for radiotherapy of cancer was explored by Battermann et al. [31], who measured
65 the response of pulmonary metastases to fast neutron single and multiple dose fractions. There are several other articles dealing with the biological effects induced by neutrons but for the sake of brevity they will be cited without further comments [32, 33, 34]. The Dual Radiation Action Theory (DRAT) [35] has been the most successful model to explain the effect of ionizing radi-
70 ation in living cells. It supposes that there are sublethal lesions that, if not repaired by the cell, may interact together for inducing more severe damages such as chromosome aberrations. These aberrations can lead to cell death or neoplastic transformation. Several radiobiological models have been based on

this theory, for instance, the Linear-Quadratic model [36, 37]. Some biophysical
75 models developed for describing the damage induced by ionizing radiation use
the double-strand break (DSB) as the possible sublethal damage. This is the
case in the Microdosimetric-Kinetic Model (MKM) [38], where a mathematical
formalism was developed to link microdosimetric quantities to radiobiological
effects. Another example is the BIANCA model, developed by Ballarini et al.
80 [39], which starts from a DSB spatial distribution according to the incident ra-
diation quality, yet, the DSB induction process is not explicitly simulated. The
Local Effect Model of Elsasser et al. [40] assumes that the lethality of radiation
depends on its capacity for producing a high density of double-strand breaks,
even from clusters of single-strand breaks within a genomic distance of 25 base-
85 pairs. However, they do not account for the interaction of DSBs, leading to
more complex lesions such as chromosome aberrations. The purpose of this
study is to investigate the RBE of fast neutrons using an approach based on the
combination of Monte Carlo (MC) simulations and an atomic resolution model
of human genetic material. A model recently developed by our group has been
90 used [41]. This model goes a step further and simulates the generation of DSB
explicitly and accounts for the interaction of these DSBs leading to chromosome
aberrations. This work aims at deriving RBE values from direct DSB induction.
For this purpose, dose-effect curves were constructed by accounting for lethal
damages induced by the combination of two DSBs. These curves were fitted with
95 a linear-quadratic model, from which the parameter α was extracted for each
radiation quality. Later, this parameter was used for determining the so-called
maximum RBE or zero-dose RBE (RBE_{max}). It is well known that neutrons
produce heavy secondary particles, which can ionize the medium and produce
a complex spatial distribution of energy deposits [42, 43]. To our knowledge,
100 this is the first time that fast neutron RBE has been determined using this ap-
proach, that is, starting from the simulation of the radiation-DNA interaction
and going up to the formation of chromosome aberrations.

2. Methods

2.1. Irradiation setup and DNA model

105 Fast monoenergetic neutrons with energies of 0.1, 0.2, 0.37, 0.4, 0.5, 0.7, 1, 2, 5, 7, 10, 12, and 14 MeV were used as primary particles. These energies are of interest in fast neutron therapy of cancer and for radiation protection. The corresponding minimum and maximum mean free paths are approximately 0.99 cm and 9.73 cm, respectively. ^{60}Co radiation was also simulated because
110 it was used as the reference quality for RBE determination. The geometry of simulations consisted in a sphere with 1.0 cm radius. This sphere was filled with $1.0 \text{ g}\cdot\text{cm}^{-3}$ water. Primary particles were shot from the surface of the sphere towards its center. Initial neutron and photon positions were sampled uniformly on the sphere surface. Fig. 1 shows the described setup. The re-
115 gion of interest (ROI) is a $3 \mu\text{m}$ -side cube placed at the center of the sphere. This ROI contains the DNA geometrical model, which has been described in detail elsewhere [41]. In brief, a cell nucleus was modeled as a cube with approximately 3 micron-side, where straight chromatin fiber segments are aligned parallel to each other. This simplification allowed getting a squared ROI base
120 and a relatively simple method for finding the chromatin fiber hit by the energy deposition. The ROI was filled with 98×98 30-nm chromatin fibers, where the explicit position of each atom of the DNA molecule was accounted for [44]. The whole nucleus contains 5.47×10^9 base pairs (bp). The target volume for DNA break induction was defined as the union volume of all the atoms contained in
125 a sugar-phosphate group. It is approximately 0.13 nm^3 [44]. Simulations were carried out with the *Geant4* (v.10.2) [45] MC code. Specifically, the subpackage *Geant4-DNA* was used [46, 47, 48, 49]. In this energy range and for this target material, neutrons can produce particles from hydrogen up to fluorine. These particles later produce a complex cascade of electrons and photons. This im-
130 posed a challenge when defining the *Geant4* physical models to be used in these simulations. The simulation world was divided into two regions, namely, the ROI and the rest. Since the whole genetic material model was placed into the

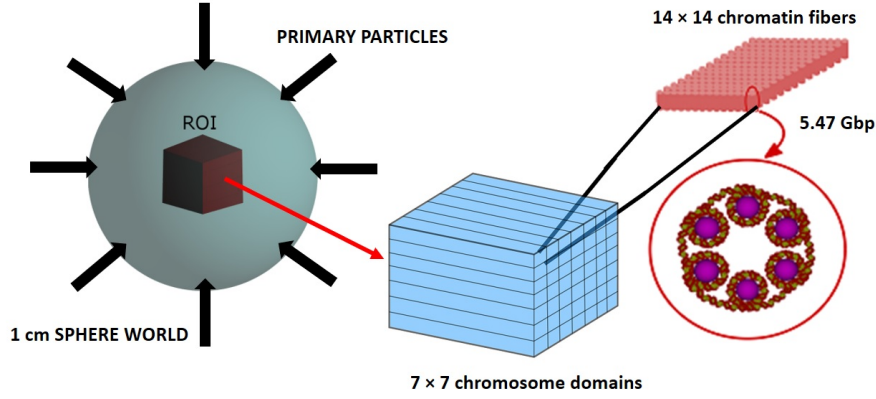


Figure 1: Irradiation setup for neutrons and photons. Not to scale.

ROI, transport of charged particles inside this region was carried out with the Geant4-DNA models, at least for those species included in such models. Outside
 135 the ROI, standard models were used both for charged and uncharged particles. Table 1 shows the physical models used in each region. It is worth mentioning that there is no model overlap in the different regions. Photon transport in the Geant4-DNA default physics list (referred to as "G4EmDNAPhysics"), which was used in the ROI, uses the Livermore cross-section model.

Table 1: Geant4 physical models used in each region.

Particle	Entire world	Inside ROI	Outside ROI
Neutrons	QGSP_BERT_HP	-	-
Electrons	-	G4EmDNAPhysics	G4EmStandardPhysics
Photons	-	G4EmDNAPhysics	G4EmStandardPhysics
Protons and Helium species	-	G4EmDNAPhysics	G4IonPhysics
C, N, O	-	G4EmDNAPhysics	G4IonPhysics
F	G4IonPhysics	-	-

140 *2.2. Calculation of RBE.*

The RBE is defined as a function of the biological endpoint and dose or dose per fraction. One of these endpoints is DSB induction [22, 50], which was used in this work. DSB yields were calculated for all neutron energies and ^{60}Co γ -rays. A single-strand break (SSB) was counted if a target was hit with an energy transfer greater than 8 eV, which is similar to the minimum water excitation energy. It is well known that even lower energy transfers (down to ~ 1 eV) can induce an SSB [51]. However, it was decided not to follow electrons below 8 eV due to the uncertainties associated with Monte Carlo simulations at such low energies. Since we are determining a relative quantity, RBE, a small variation of this parameter should not have a great impact in this case. DSB was counted if two SSBs in opposite strands were found at a distance less than 10 bp. This is a widespread practice in this field [52, 53]. Then, DSB yields were used for estimating the RBE as follows,

$$RBE_{DSB} = \frac{Y_{DSB-neutron}}{Y_{DSB-^{60}Co}} \quad (1)$$

where $Y_{\text{DSB-neutron}}$ and $Y_{\text{DSB-}^{60}\text{Co}}$ are the direct DSB yields for neutrons and ^{60}Co photons, respectively. The direct to indirect damage yield ratio depends on the radiation quality. Since this work only accounts for the direct damage, reported RBE based on the DSB yield should be taken as rough estimates.

145 We have also estimated neutron RBE following a numerical approach recently developed by Tello et al. [41]. In this approach, DSBs are taken as sublethal lesions that can interact with each other to induce lethal chromosomal aberrations. Each DSB is labeled according to the primary particle, and its position is recorded. Later, a repair probability of 55 % is applied to the whole
 150 DSB population [54]. Afterwards, a Gaussian distribution with a characteristic distance of 600 nm is used for sampling the number of lethal lesions formed from the interaction of two DSBs. The DNA model is irradiated with doses from 1 to 5 Gy so that dose-effect curves could be obtained, from which the well-known α and β parameters were extracted [55, 56]. As said in our previous work [41],
 155 the quadratic curve must have two zeros because the number of lethal lesions

induced by independent tracks has to be zero at $D=0$ Gy and $D=D_0$, where D_0 is the one-track dose. Thus, this quadratic component was fitted using the following equation

$$N_\beta = \beta D(D - D_0). \quad (2)$$

Then the final equation for the number of lethal lesions is

$$N_{LL} = (\alpha - \beta D_0)D + \beta D^2 \quad (3)$$

$$= \alpha' D + \beta D^2, \quad (4)$$

160 where α' is the parameter used for determining the RBE of the neutrons.

Each simulation was divided into 10 batches so that a statistical analysis could be performed. Each batch included about 100 000 primary neutrons, depending on the incident neutron energy. Then, the so-call maximum RBE was determined as

$$RBE_{max} = \frac{\alpha'_{neutron}}{\alpha'_{60Co}}, \quad (5)$$

where $\alpha'_{neutron}$ and α'_{60Co} are the α' parameters for the radiation qualities in question. This ratio is also known as the zero-dose RBE.

3. Result and Discussion

3.1. ^{60}Co , direct SSB and DSB yield

165 Results for ^{60}Co photons are very important in this work, since this quality is used as reference for determining RBE. Table 2 compares the direct SSB and DSB yields obtained for this quality in this study and other similar works that used atomic DNA models. As can be observed in this table, SSB yields are very disperse, going from 28.79 $(10^9 Gy.bp)^{-1}$ to 100 $(10^9 Gy.bp)^{-1}$. SSB
170 yield depends on the energy threshold and the size of the atoms conforming the DNA. This study has the least threshold energy, 8 eV. Consequently, it has the highest SSB yield. However, DSB yield is more important when talking

about RBE. Values from Bernal et al. [57], Tajik et al. [58], and this study are very consistent. The DSB yield reported by Friedland et al. [59] is far from those reported by Tajik et al. [58] and ours. Friedland et al. used two van der Waals radii around each sugar-phosphate atom to conform the target and a damage threshold of 10.79 eV. In our model, only one radius was used. Most likely, the greater target volume used by those authors is the main reason for their higher DSB yield. The DSB yield obtained in this work is closer to that obtained in our previous work [22] than to that reported by Friedland et al. [59], probably because the same MC code, atom sizes, and DSB definition were used in our works. It should be also noticed that Friedland et al. [59] obtained more DSB per SSB than our works, which can be attributed to the different physical models used in the MC codes in question.

Table 2: ^{60}Co SSB and DSB yields. Uncertainties represent one standard deviation of the mean.

Monte Carlo code	Source	Geometry	Size(vdW^1 units)	SSB $(10^9 \text{Gy} \cdot \text{bp})^{-1}$	DSB $(10^9 \text{Gy} \cdot \text{bp})^{-1}$	SSB threshold energy (eV)
PARTRAC Friedland et al. [59]	^{60}Co γ rays	Atomic	2	92 ± 5	4.9 ± 0.1	10.79
Geant4-DNA Zabihi et al. [22]	Secondary electrons from ^{60}Co γ -rays	Atomic	1	73.506 ± 0.006	3.80 ± 0.08	10.79
Geant4-DNA This study	^{60}Co γ rays	Atomic	1	100.0 ± 0.3	3.63 ± 0.05	8.0

3.2. The α and β parameters

It should be remarked that our model has four parameters, namely, the energy threshold for a single-strand break induction (8.0 eV), the maximum genomic distance between two single-strand breaks for the induction of a double-strand break, the DSB repair probability, and the characteristic distance for the interaction of two sublethal damages leading to a lethal damage. The values chosen for these parameters are the same as those used for ions in our previous work [41] since most of them probably do not depend on the incident radiation quality. Figs. 2a and 2b show the number of lethal lesions induced through the so-called linear and quadratic mechanisms, from which the α and β parameters

195 were determined. As expected, Fig. 2a shows that the slope (α) of the ^{60}Co curve is much lower than that of neutrons. This is due to the relatively low probability for a single photon track to produce a two-DSB interaction. Furthermore, a slight tendency to saturation is observed in the curves shown in this figure, mainly for the 0.2 MeV case. This behavior was discussed in our previous
 200 publication [41]. As the dose increases, primary particle fluence also increases, so the DSB has a greater probability to interact with another DSB induced by independent tracks. Thus, the increment in the number of intratrack interactions with dose slows down so that the behavior departs from a straight line. This effect is also influenced by the characteristic distance for DSB interactions.

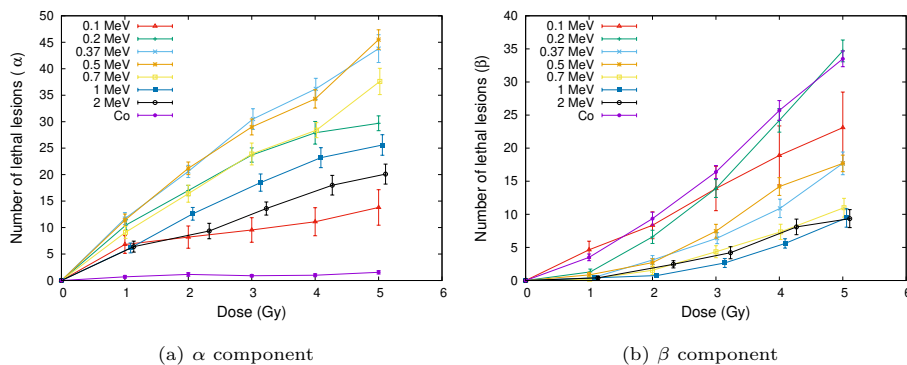


Figure 2: Number of lethal lesions as a function of dose for intra and intertrack mechanisms.

205

For protons, we observed that this threshold dose increases as the LET increases. At a given dose, fluence is inversely proportional to primary particle LET so higher doses are needed to observe the increment in the intertrack effect in detriment of intratrack interactions. For neutrons the analysis is much more
 210 difficult since there are heavy charged secondary particles involved and LET is not enough to explain this behavior, not even that of RBE as a function of the incident energy. It can also be noticed that the slope of this curve increases as the incident neutron energy increases from 0.1 MeV, reaching a maximum for approximately 0.37 MeV, then decreases. Thus, it could be expected that

215 the RBE shows a maximum in this impact energy interval. Fig. 2b shows
the quadratic behavior of the intertrack interactions for the incident energies
in question. Some curves look such as quasi-straight lines, which means that
intertrack effects are weak when compared to intratrack DSB interactions. This
is an expected behavior for high LET particles. The authors are aware that
220 the current model setup leads to an overestimation of lethal lesion yields when
compared to high LET chromosome aberration yields. However, the scope of
this work is the estimation of RBE for neutrons. The other crucial point here
is that lower lesion yields produce too high uncertainties when determining α
parameters and so RBE. Then, it was decided to keep relatively high lethal
225 lesion yields to get acceptable uncertainties and, at the same time, good RBE
estimates were obtained.

3.3. Neutron RBE_{max}

Fig. 3 depicts the behavior of RBE_{max} as a function of neutron incident
energy, obtained using eq. 5. We had problems for extending α -based calcu-
230 lations above 2 MeV. Indeed, the Geant4-DNA package can only track heavy
ions down to 0.5 MeV/u so ^{12}C , ^{13}C , and ^{16}O ions produced by the impact of
neutrons on the water molecule could not be followed below this energy. Then,
some of these ions were stopped at this energy inside the ROI, which led to
very high absorbed doses. This did not allow us to construct the curve for
235 neutron energies above 2 MeV, where the production of the mentioned ions is
important. Previously published experimental results are also shown for com-
parison purposes. These experiments were carried out for different biological
endpoints, reference radiation qualities and cell lines. The reader should keep
in mind that data on cell survival should not be directly compare to our results
240 based on chromosome aberrations. However, the authors decided to include
cell survival data for sake of completeness. It is very difficult to compare these
results together due to the diversity of endpoints and the lack of uncertainties
in many of these works. Moreover, even for experiments carried out in similar
conditions, very different results were obtained. However, the general behavior

245 of the RBE as a function of the incident neutron energy seems to be the same.
There is a maximum at approximately 0.4 MeV and then the RBE decreases as
the incident energy increases. Our results agree rather well with those reported
by Miller et al. [60]. However, it should be remarked that their reference qual-
ity (250 X-rays) should produce an RBE slightly lower than that when using
250 ^{60}Co . The results published by Schmid et al. [21] were obtained in conditions
similar to our simulation. They counted chromosome aberrations and used the
same reference quality. Even though, their RBE values are much higher than
ours, and they present very large uncertainties. Tanaka et al. [27] reported
 RBE_{max} for chromosome aberrations, which are lower than ours are but seem
255 to follow the same trend. The last value of this series is similar to that obtained
by McNally et al. [61] but a rigorous comparison cannot be done since they
used different cell lines and reference radiation quality. The results of Pandita
et al. [28] are closer to ours, with some values within the uncertainty of our
calculations. It should be clarified that Pandita et al. reported the α parameter
260 for three kinds of chromosome aberrations, for ^{60}Co and neutrons as well. We
summed up all the α parameters to get one that represents all types of aberra-
tions. They used ^{137}Cs as the reference radiation, which should yield a similar
RBE to those obtained with ^{60}Co . Finally, the results reported by Suzuki [62],
Higgins et al. [63] and Ngo et al. [64] seem to follow the same trend described
265 by Pandita et al. and Schmid et al. It should be remarked that these three
researchers used the same biological endpoint, reference radiation, and cell line.
Although it cannot be rigorously confirmed, our results seem to head in the
direction of these points. Table 4 summarizes the endpoint, the position of the
maximum RBE as a function of the incident neutron energy, and the reference
270 quality used in several works and ours. We decided to include other reference
qualities in this table because the position of RBE_{max} should not depend on
this quality. Our results show RBE_{max} at 0.37-0.4 MeV, which agrees very well
with the corresponding values given in Table 4.

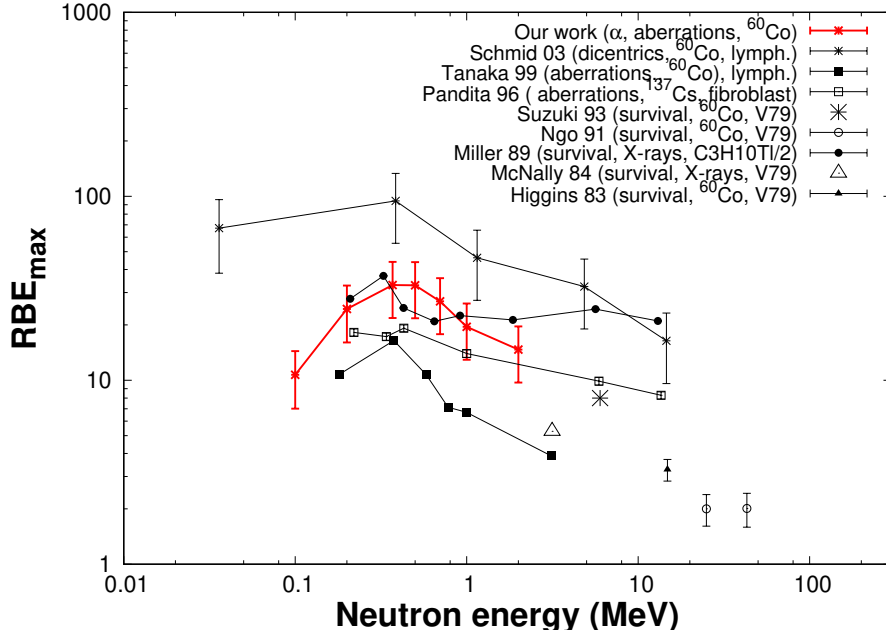


Figure 3: RBE_{max} as a function of the incident neutron energy determined based on the α parameter. Values reported in several experiments are also shown for comparison purposes.

3.4. Neutron RBE_{DSB}

275 Table 3 shows absolute SSB and DSB yields across the neutron energy range. The reader should take these values as rough estimations on direct damage yields because our work aims at estimating RBE, a relative quantity, instead of absolute damage yields.

Table 3: Neutron direct SSB and DSB yields. Uncertainties represent one standard deviation of the mean.

Energy (MeV)	0.1	0.2	0.37	0.5	0.7	1
SSB ($10^9 Gybp$) ⁻¹	188.9 ± 0.2	176.9 ± 0.3	159.6 ± 0.3	154.5 ± 0.2	149.4 ± 0.3	112.5 ± 0.3
DSB ($10^9 Gybp$) ⁻¹	19.3 ± 0.2	20.9 ± 0.3	19.6 ± 0.2	19.3 ± 0.2	16.1 ± 0.2	10.8 ± 0.2
Energy (MeV)	2	5	7	10	12	14
SSB ($10^9 Gybp$) ⁻¹	117.8 ± 0.3	108.0 ± 0.8	97.3 ± 0.8	83.1 ± 0.7	74.5 ± 0.6	25 ± 1
DSB ($10^9 Gybp$) ⁻¹	10.4 ± 0.4	6.0 ± 0.6	3.5 ± 0.3	3.0 ± 0.4	3.1 ± 0.4	2.8 ± 0.8

280 Fig. 4 shows the RBE obtained in this work using the production of DSB as an endpoint. However, it should be remarked that DSB yield and DSB cluster

yield are different quantities, but it was decided to show DSB-related yields in the same plot. Similar results reported by other authors are also shown. Again, the results are very dispersed. In this case, we could go up to 14 MeV. Thus, as heavy secondary charged particles could not be followed down to energies
285 below 0.5 MeV/u, it can be said that our values should underestimate RBE for neutron energies above ~ 2 MeV, where the production of these particles is more important. Notice that these results go even below 1 for energy of approximately 10 MeV, but they are comparable to 1 within the uncertainty. Below 2 MeV, the tendency of our results is similar to that shown by the experimental
290 values reported by Tanaka et al. [27], yet an important underestimation is observed. Despite that Stewart et al. [24] and Baiocco et al. [23] used the same endpoint, DSB cluster, the difference is about fivefold. Stewart's results are unable to reproduce the rapid decrease of RBE above ~ 0.4 MeV, as observed for the other results. We observe that, for energies up to approximately 1 MeV,
295 results show a similar trend as our previous calculations [22]. Above 1 MeV, the RBE values of our data are less than the previous work. This was due to the fact that, most likely all secondary particles couldn't reach to the nucleus. Therefore, their deposited energy and damages are lesser in comparison with our previous study. It should be pointed out that the comparison with other works
300 based on simulations should be seen as a verification of our results, instead of a confirmation of our model. Unfortunately, only one experimental data series was found in this case so the comparison with these data should not be seen as conclusive.

RBE associated with neutrons is mainly determined by the secondary heavy
305 charged particles produced by their interaction with water, in this case. Zabihi et al. [22] showed the relative production of secondary ions, both by elastic and inelastic interaction of neutrons with water. On the one hand, interaction with hydrogen is almost dominated by elastic collisions which produce secondary protons, the most abundant secondary particles in this situation. This can be
310 observed in Table 5. This cross-section decreases continuously as the neutron energy increases. On the other hand, cross-sections for oxygen are dominated

Table 4: Position of RBE_{max} as a function of the incident neutron energy. Our results and those reported by similar works are shown.

Reference	Method	Parameter+endpoint	Pos. of RBE_{max} (MeV)	reference radiation
Baiocco et al. (16) [23]	Theor.	DSB cluster yield	0.555	220 kV X-rays
Stewart et al. (15) [24]	Theor.	DSB cluster yield	0.1	^{60}Co γ -rays
Schmid et al. (03)[21]	Exp.	α , dicentric	0.385	^{60}Co γ -rays
Schmid et al. (03)[21]	Exp.	α , dicentric	0.385	220 kV X-rays
Tanaka et al. (99)[27]	Exp.	α , dicentric	0.37	^{60}Co γ -rays
Miller et al. (89)[60]	Exp.	α , survival	0.35	250 kV X-rays
Miller et al. (89)[60]	Exp.	α , neoplastic transformation	0.35	250 kV X-rays
Pandita et al. (96)[28]	Exp.	α , dicentric+centric rings	0.43	^{137}Cs γ -rays
Pandita et al. (96)[28]	Exp.	α , inters. deletions+acentric rings	0.22 and 0.43	^{137}Cs γ rays
Pandita et al. (96)[28]	Exp.	α , terminal deletions	0.34	^{137}Cs γ -rays
Zabihi et al. (19)[22]	Theor.	DSB yield	0.2	^{60}Co γ -rays
This work (α)	Theor.	α for DSB interactions	0.37-0.4	^{60}Co γ -rays
This work (DSB)	Theor.	DSB yield	0.2	^{60}Co γ -rays

by elastic collisions up to approximately 7 MeV. Above this energy, the importance of inelastic cross-sections increases. Protons are the most abundant secondary particles generated by the impact of neutrons on water at energies near the RBE peak. Thus, the position of this peak can be explained looking at these particles. At 400 keV, neutrons transfer to protons an average energy of approximately 200 keV. At this energy, the proton range is approximately 3 μm , which is the size of a typical cell nucleus. In this situation, the energy that a proton can transfer to a cell nucleus is maximized and so the damage yield.

Neutrons with energies below 400 keV produce protons with range comparable to the cell nucleus dimensions but, evidently, the total energy deposited into the nucleus would be lower. Neutrons with higher energies, eject protons with higher energies and lower stopping powers so the dose into the nucleus would also be lower than that in the 400 keV case. The reader should notice that our cell nucleus model has a characteristic dimension of approximately 3 μm . Above 5-7 MeV, both fractions of light and heavy ions increase very fast which may explain the further increase of RBE above approximately 5 MeV, as shown by the results of Ref. [23], [60], and [24]. This is just the energy threshold for α -particle production through neutron-water collision. In this energy interval heavy ions are likely more important than the ions around the RBE peak are. Fluorine can be indirectly produced in this context by the reaction $^{16}\text{O}(\text{p},\gamma)\text{F}^{17}$.

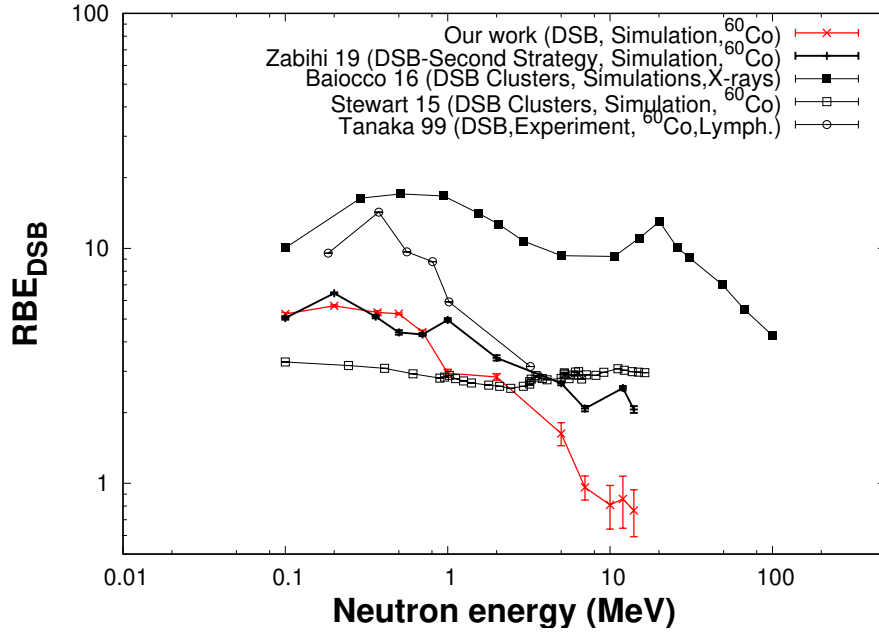


Figure 4: RBE_{DSB} as a function of the incident neutron energy determined in this work using DSB yield as endpoint. Similar results extracted from the references shown in Table 4 are also shown.

4. Conclusions

A fully numerical and mechanistic biophysical model that accounts for the production of lethal damage from the interaction of two sublethal lesions in-

335 sults has been used in this work for estimating the RBE for neutrons in a wide energy range. DSB was taken as sublethal damage. This model starts from the Monte Carlo simulation of the incoming particles during their interactions with liquid water. Only four parameters were used in this case. It has been shown that the approach based on the DSB interaction is able to reproduce

340 the general behavior of fast neutron RBE well. Furthermore, the corresponding results agree well with some experimental results and reproduce the RBE peak position, which has been reported in several experimental works. However, using DSB as the endpoint does not lead to so satisfactory results, since they do not show the RBE peak clearly. In addition, they tend to underestimate

Table 5: Fraction of the number of secondary heavy charged particles produced by the impact of neutrons with water. "Light ions" means Helium (only produced above ~ 5 MeV) species and deuteron. "Heavy ions" includes carbon, oxygen, and fluorine species.

Energy (MeV)	Protons (%)	Light ions (%)	Heavy ions (%)	All ions(%)
0.1	89.212	0.010	10.778	10.788
0.2	87.373	0.009	12.618	12.627
0.3	85.554	0.007	14.438	14.446
0.37	82.667	0.006	17.326	17.333
0.5	77.236	0.006	22.759	22.764
0.7	80.609	0.006	19.385	19.391
1	63.228	0.006	36.766	36.772
2	78.651	0.011	21.218	21.349
5	74.241	2.189	21.338	25.759
7	72.743	1.669	23.570	27.257
10	57.746	5.873	36.381	42.254
12	48.556	6.411	45.033	51.444
14	45.759	7.577	46.664	54.241

345 RBE for neutron energies above approximately 5 MeV due to the impossibility
of following heavy secondary ions below 0.5 MeV/u. Finally, it should be re-
marked that this model used the same parameters for all the radiation qualities
studied so far, including our previous work on ions. This is a demonstration
of the robustness of our model, despite its simplicity. Some improvements will
350 be introduced in the model, mainly for adjusting the sublethal repair fraction
which may depend on the radiation quality. In addition, indirect effects will also
be included so that DSB cluster formation could be used instead of a single DSB.

5. Acknowledgments

355 M. A. Bernal thanks the *Conselho Nacional para o Desenvolvimento Científico
e Tecnológico (CNPq)*, Brazil, for financing his research activities through the

project 306775/2015-8. He also acknowledges the support received from the FAPESP foundation in Brazil, through the 2011/51594-2, 2015/21873-8, and 2018/15316-7 projects.

360 **References**

References

- [1] A. V. Solov'yov, E. Surdutovich, E. Scifoni, I. Mishustin, W. Greiner, Physics of ion beam cancer therapy: A multiscale approach, *Phys. Rev. E* 79 (2009) 011909.
- 365 [2] D. Viduna, K. Hinsin, G. Kneller, Influence of molecular flexibility on DNA radiosensitivity: a simulation study, *Physical Review E* 62 (3) (2000) 3986.
- [3] M. B. Hahn, S. Meyer, H.-J. Kunte, T. Solomun, H. Sturm, Measurements and simulations of microscopic damage to DNA in water by 30 keV electrons: A general approach applicable to other radiation sources and biological targets, *Physical Review E* 95 (5) (2017) 052419.
- 370 [4] E. Nováková, L. Vyšín, T. Burian, L. Juha, M. Davidková, V. Múčka, V. Čuba, M. E. Grisham, S. Heinbuch, J. J. Rocca, Breaking DNA strands by extreme-ultraviolet laser pulses in vacuum, *Physical Review E* 91 (4) (2015) 042718.
- 375 [5] T. Straume, G. Rugel, A. A. Marchetti, W. Ruhm, G. Korschinek, J. E. McAninch, K. Carroll, S. Egbert, T. Faestermann, K. Knie, R. Martinelli, A. Wallner, C. Wallner, Measuring fast neutrons in Hiroshima at distances relevant to atomic-bomb survivors, *Nature* 424 (6948) (2003) 539–542.
- 380 [6] T. Shibata, M. Imamura, S. Shibata, Y. Uwamino, T. Ohkubo, S. Satoh, N. Nogawa, H. Hasai, K. Shizuma, K. Iwatani, M. Hoshi, T. Oka, A method to estimate the fast-neutron fluence for the Hiroshima atomic bomb, *Journal of the Physical Society of Japan* 63 (10) (1994) 3546–3547.

- [7] W. Rühm, L. Walsh, M. Chomentowski, Choice of model and uncertainties of the gamma-ray and neutron dosimetry in relation to the chromosome aberrations data in Hiroshima and Nagasaki, *Radiation and environmental biophysics* 42 (2) (2003) 119–128. 385
- [8] R. Sakata, E. J. Grant, K. Furukawa, M. Misumi, H. Cullings, K. Ozasa, R. E. Shore, Long-term effects of the rain exposure shortly after the atomic bombings in Hiroshima and Nagasaki, *Radiation research* 182 (6) (2014) 599–606. 390
- [9] A. Burlon, A. Kreiner, A. Valda, D. Minsky, H. Somacal, M. Debray, P. Stoliar, Optimization of a neutron production target and a beam shaping assembly based on the ${}^7\text{Li}(p, n){}^7\text{Be}$ reaction for BNCT, *Nuclear Instruments and Methods in Physics Research Section B: Beam Interactions with Materials and Atoms* 229 (1) (2005) 144–156. 395
- [10] T. E. Blue, B. W. Wehring, S. J. Briggs, C. S. Wepprecht, J. S. Durham, J. W. Blue, Dosimetry in fast-neutron therapy by automatic readout of CR-39, *Nuclear Instruments and Methods in Physics Research Section B: Beam Interactions with Materials and Atoms* 14 (4-6) (1986) 589–595.
- [11] J. Smathers, L. Myers, Neutron therapy and dosimetry at the UCLA neutron therapy facility, *Nuclear Instruments and Methods in Physics Research Section B: Beam Interactions with Materials and Atoms* 24 (1987) 1077–1081. 400
- [12] M.-A. Timoshchuk, P. Dekker, D. S. Hippe, U. Parvathaneni, J. J. Liao, G. E. Laramore, J. K. Dillon, The efficacy of neutron radiation therapy in treating salivary gland malignancies, *Oral oncology* 88 (2019) 51–57. 405
- [13] S. K. Schaub, R. D. Stewart, G. A. Sandison, T. Arbuckle, J. J. Liao, G. E. Laramore, J. Zeng, R. Rengan, Y. D. Tseng, N. A. Mayr, et al., Does neutron radiation therapy potentiate an immune response to merkel cell carcinoma?, *International Journal of Particle Therapy* 5 (1) (2018) 183–195. 410

- [14] T. Imaoka, M. Nishimura, K. Daino, A. Hosoki, M. Takabatake, T. Kokubo, K. Doi, K. Showler, Y. Nishimura, H. Moriyama, et al., Age modifies the effect of 2-MeV fast neutrons on rat mammary carcinogenesis, *Radiation research* 188 (4) (2017) 419–425.
- [15] F. Wagner, B. Loeper-Kabasakal, H. Breitzkreutz, Neutron medical treatment of tumours a survey of facilities, *Journal of Instrumentation* 7 (03) (2012) C03041.
- [16] O. Kozak, A. Shvedov, O. Trembach, O. Morus, The role of heavy ions in fast neutron therapy, in: *International Scientific and Practical Conference World science, Vol. 1, ROST, 2018*, pp. 10–15.
- [17] M. Bauchinger, L. Koester, E. Schmid, J. Dresch, S. Streng, Chromosome aberrations in human lymphocytes induced by fission neutrons, *International Journal of Radiation Biology and Related Studies in Physics, Chemistry and Medicine* 45 (5) (1984) 449–457.
- [18] L. Gray, J. Read, Treatment of cancer with fast neutrons, *Nature* 152 (1943) 53.
- [19] L. H. Gray, A. Conger, M. Ebert, S. Hornsey, O. Scott, The concentration of oxygen dissolved in tissues at the time of irradiation as a factor in radiotherapy, *The British journal of radiology* 26 (312) (1953) 638–648.
- [20] R. Stone, Neutron therapy and specific ionization., *The American Journal of Roentgenology and radium therapy* 59 (6) (1948) 771–785.
- [21] E. Schmid, D. Schlegel, S. Guldbakke, R.-P. Kapsch, D. Regulla, RBE of nearly monoenergetic neutrons at energies of 36 keV–14.6 MeV for induction of dicentric chromosomes in human lymphocytes, *Radiation and environmental biophysics* 42 (2) (2003) 87–94.
- [22] A. Zabihi, S. Incerti, Z. Francis, G. Forozani, F. Semsarha, A. Moslehi, P. Rezaeian, M. A. Bernal, Computational approach to determine the relative biological effectiveness of fast neutrons using the Geant4-DNA toolkit

- 440 and a DNA atomic model from the protein data bank, *Physical Review E*
99 (5) (2019) 052404.
- [23] G. Baiocco, S. Barbieri, G. Babini, J. Morini, D. Alloni, W. Friedland,
P. Kunderát, E. Schmitt, M. Puchalska, L. Sihver, et al., The origin of
neutron biological effectiveness as a function of energy, *Scientific Reports*
445 6 (2016).
- [24] R. D. Stewart, S. W. Streitmatter, D. C. Argento, C. Kirkby, J. T. Goor-
ley, G. Moffitt, T. Jevremovic, G. A. Sandison, Rapid mcnp simulation of
DNA double strand break (DSB) relative biological effectiveness (RBE) for
photons, neutrons, and light ions, *Physics in medicine and biology* 60 (21)
450 (2015) 8249.
- [25] A. Ottolenghi, G. Baiocco, V. Smyth, K. Trott, The ANDANTE project: a
multidisciplinary approach to neutron RBE, *Radiation protection dosime-
try* 166 (1-4) (2015) 311–315.
- [26] E. Schmid, D. Regulla, S. Guldbakke, D. Schlegel, M. Bauchinger, The
455 effectiveness of monoenergetic neutrons at 565 keV in producing dicen-
tric chromosomes in human lymphocytes at low doses, *Radiation research*
154 (3) (2000) 307–312.
- [27] K. Tanaka, N. Gajendiran, S. Endo, K. Komatsu, M. Hoshi, N. Ka-
mada, Neutron energy-dependent initial DNA damage and chromosomal
460 exchange, *Journal of radiation research* 40 (SUPPL) (1999) S36–S44.
- [28] T. K. Pandita, C. R. Geard, Chromosome aberrations in human fibroblasts
induced by monoenergetic neutrons. i. relative biological effectiveness, *Ra-
diation research* 145 (6) (1996) 730–739.
- [29] R. C. Miller, S. A. Marino, S. G. Martln, K. Komatsu, C. R. Geard, D. J.
465 Brenner, E. J. Hall, Neutron-energy-dependent cell survival and oncogenic
transformation, *Journal of Radiation Research* 40 (Suppl) (1999) S53–S59.
URL <http://dx.doi.org/10.1269/jrr.40.S53>

- [30] H. Warendius, J. Down, RBE of fast neutrons for apoptosis in mouse thymocytes, *International journal of radiation biology* 68 (6) (1995) 625–629.
- 470 [31] J. J. Battermann, K. Breur, G. A. Hart, H. A. Van Peperzeel, Observations on pulmonary metastases in patients after single doses and multiple fractions of fast neutrons and Cobalt-60 gamma rays, *European Journal of Cancer* (1965) 17 (5) (1981) 539–548.
- [32] T. Blue, N. Gupta, J. Woollard, A calculation of the energy dependence of the RBE of neutrons, *Physics in Medicine and Biology* 38 (12) (1993) 1693.
- 475 [33] M. Spothem-Maurizot, M. Charlier, R. Sabbattier, DNA radiolysis by fast neutrons, *International journal of radiation biology* 57 (2) (1990) 301–313.
- [34] E. J. Hall, J. K. Novak, A. M. Kellerer, H. H. Rossi, S. Marino, L. J. Goodman, RBE as a function of neutron energy: I. experimental observations, *Radiation Research* 64 (2) (1975) 245–255.
- 480 [35] A. M. Kellerer, H. H. Rossi, The action of dual radiation action, *Current Topics in Radiation Research Quarterly* 8 (1972) 85–158.
- [36] K. Chadwick, H. Leenhouts, A molecular theory of cell survival, *Physics in Medicine & Biology* 18 (1) (1973) 78.
- 485 [37] S. J. McMahon, The linear quadratic model: usage, interpretation and challenges, *Physics in Medicine & Biology* 64 (1) (2018) 01TR01.
- [38] R. B. Hawkins, A microdosimetric-kinetic theory of the dependence of the RBE for cell death on LET, *Medical Physics* 25 (7) (1998) 1157–1170.
- 490 [39] J. J. Tello Cajiao, M. P. Carante, M. A. Bernal Rodriguez, F. Ballarini, Proximity effects in chromosome aberration induction by low-LET ionizing radiation, *DNA Repair* 58 (2017) 38–46.
- [40] T. Elsässer, M. Scholz, Cluster effects within the local effect model, *Radiation Research* 167 (3) (2007) 319–329.

- 495 [41] J. J. Tello, M. A. Bernal, S. Incerti, Z. Francis, H. N. Tran, Numerical insight into the dual radiation action theory, *Physica Medica* 43 (2017) 120-126.
- [42] R. S. Caswell, J. J. Coyne, Interaction of neutrons and secondary charged particles with tissue: Secondary particle spectra, *Radiation research* 52 (3) 500 (1972) 448–470.
- [43] D. Bewley, Calculated let distributions of fast neutrons, *Radiation research* 34 (2) (1968) 437–445.
- [44] M. A. Bernal, D. Sikansi, F. Cavalcante, S. Incerti, C. Champion, V. Ivanchenko, Z. Francis, An atomistic geometrical model of the B-DNA 505 configuration for DNA-radiation interaction simulations, *Computer Physics Communications* 184 (12) (2013) 2840–2847.
- [45] S. Agostinelli, J. Allison, K. a. Amako, J. Apostolakis, H. Araujo, P. Arce, M. Asai, D. Axen, S. Banerjee, G. Barrand, et al., Nuclear instruments and methods in physics research section A: Accelerators, Spectrometers, 510 Detectors and Associated Equipment 506 (3) (2003) 250–303.
- [46] M. Bernal, M. Bordage, J. Brown, M. Davidková, E. Delage, Z. El Bitar, S. Enger, Z. Francis, S. Guatelli, V. Ivanchenko, et al., Track structure modeling in liquid water: A review of the Geant4-DNA very low energy extension of the Geant4 Monte Carlo simulation toolkit, *Physica Medica* 515 31 (8) (2015) 861–874.
- [47] S. Incerti, I. Kyriakou, M. Bernal, M. Bordage, Z. Francis, S. Guatelli, V. Ivanchenko, M. Karamitros, N. Lampe, S. B. Lee, et al., Geant4-DNA example applications for track structure simulations in liquid water: a report from the Geant4-DNA project, *Medical physics* 45 (8) (2018) e722–520 e739.
- [48] S. Incerti, G. Baldacchino, M. Bernal, R. Capra, C. Champion, Z. Francis, P. Guèye, A. Mantero, B. Mascialino, P. Moretto, et al., The Geant4-

DNA project, *International Journal of Modeling, Simulation, and Scientific Computing* 1 (02) (2010) 157–178.

- 525 [49] V. Ivanchenko, S. Incerti, Z. Francis, H. Tran, M. Karamitros, M. Bernal, C. Champion, P. Gueye, Combination of electromagnetic physics processes for microdosimetry in liquid water with the Geant4 Monte Carlo simulation toolkit, *Nuclear Instruments and Methods in Physics Research Section B: Beam Interactions with Materials and Atoms* 273 (2012) 95–97.
- 530 [50] P. Pater, G. Bäckström, F. Villegas, A. Ahnesjö, S. A. Enger, J. Seuntjens, I. El Naqa, Proton and light ion rbe for the induction of direct DNA double strand breaks, *Medical physics* 43 (5) (2016) 2131–2140.
- [51] R. Panajotovic, F. Martin, P. Cloutier, D. Hunting, L. Sanche, Effective cross sections for production of single-strand breaks in plasmid DNA by 0.1 to 4.7 eV electrons, *Radiation Research* 165 (4) (2006) 452–459.
- 535 [52] W. Friedland, P. Jacob, P. Bernhardt, H. G. Paretzke, M. Dingfelder, Simulation of DNA damage after proton irradiation, *Radiation Research* 159 (3) (2003) 401–410.
- [53] S. Meylan, S. Incerti, M. Karamitros, N. Tang, M. Bueno, I. Clairand, C. Villagrasa, Simulation of early DNA damage after the irradiation of a fibroblast cell nucleus using Geant4-DNA, *Scientific Reports* 7 (1) (2017) 11923.
- 540 [54] B. Fouladi, C. A. Waldren, B. Rydberg, P. K. Cooper, Comparison of repair of DNA double-strand breaks in identical sequences in primary human fibroblast and immortal hamster–human hybrid cells harboring a single copy of human chromosome 11, *Radiation research* 153 (6) (2000) 795–804.
- 545 [55] L. Lindborg, M. Hultqvist, Å. C. Tedgren, H. Nikjoo, Nanodosimetry and RBE values in radiotherapy, *Radiation protection dosimetry* (2015) ncv196.

- [56] M. Löbrich, P. K. Cooper, B. Rydberg, Joining of correct and incorrect
550 DNA ends at double-strand breaks produced by high-linear energy transfer
radiation in human fibroblasts, *Radiation research* 150 (6) (1998) 619–626.
- [57] M. A. Bernal, J. A. Liendo, An investigation on the capabilities of the
PENELOPE MC code in nanodosimetry., *Medical Physics* 36 (2) (2009)
620–625.
- 555 [58] M. Tajik, A. S. Rozatian, F. Semsarha, Calculation of direct effects of
 ^{60}Co gamma rays on the different DNA structural levels: a simulation
study using the Geant4-DNA toolkit, *Nuclear Instruments and Methods in
Physics Research Section B: Beam Interactions with Materials and Atoms*
346 (2015) 53–60.
- 560 [59] W. Friedland, P. Jacob, H. G. Paretzke, M. Merzagora, A. Ottolenghi,
Simulation of DNA fragment distributions after irradiation with photons,
Radiat. Environ. Biophys. 38 (1999) 39–47.
- [60] R. Miller, C. Geard, D. J. Brenner, K. Komatsu, S. A. Marino, Neutron-
energy-dependent oncogenic transformation of C3H 10LT/2 mouse cells,
565 *Radiat. Res.* 117 (1989) 114–127.
- [61] N. J. McNally, J. de Ronde, M. Hinchliffe, The effect of sequential irradiation
with X-rays and fast neutrons on the survival of V79 chinese hamster
cells, *Int J Radiat Biol* 45 (4) (1984) 301–310.
- [62] S. Suzuki, Survival of chinese hamster V79 cells after irradiation with a
570 mixture of neutrons and co-60 gamma rays: Experimental and theoretical
analysis of mixed irradiation, *Radiat. Res.* 133 (1993) 327333.
- [63] P. D. Higgins, P. M. DeLuca, D. W. Pearson, V79 survival following simultaneous
or sequential irradiation by 15-MeV neutrons and Co-60 photons,
Radiat. Res. 95 (1983) 45–56.

- ⁵⁷⁵ [64] F. Q. H. Ngo, C. Schroy, X. L. Jia, I. Kalvakolanu, W. K. Roberts, J. Blue, A. Antunez, P. D. Higgins, M. Tefft, Basic radiobiological investigations of fast neutrons, *Radiat. Res.* 128 (1991) S94-S102.